Chapter

Stimulated Scattering of Surface Plasmon Polaritons in a Plasmonic Waveguide with a Smectic A Liquid Crystalline Core

Boris I. Lembrikov, David Ianetz and Yossef Ben Ezra

Abstract

We considered theoretically the nonlinear interaction of surface plasmon polaritons (SPPs) in a metal-insulator-metal (MIM) plasmonic waveguide with a smectic liquid crystalline core. The interaction is related to the specific cubic optical nonlinearity mechanism caused by smectic layer oscillations in the SPP electric field. The interfering SPPs create the localized dynamic grating of the smectic layer strain that results in the strong stimulated scattering of SPP modes in the MIM waveguide. We solved simultaneously the smectic layer equation of motion in the SPP electric field and the Maxwell equations for the interacting SPPs. We evaluated the SPP mode slowly varying amplitudes (SVAs), the smectic layer dynamic grating amplitude, and the hydrodynamic velocity of the flow in a smectic A liquid crystal (SmALC).

Keywords: surface plasmon polariton (SPP), smectic liquid crystals, stimulated light scattering (SLS), plasmonic waveguide

1. Introduction

Nonlinear optical phenomena based on the second- and third-order optical nonlinearity characterized by susceptibilities $\chi^{(2)}$ and $\chi^{(3)}$, respectively, are widely used in modern communication systems for the optical signal processing due to their ultrafast response time and a large number of different interactions [1–5]. The second-order susceptibility $\chi^{(2)}$ exists in non-centrosymmetric media, while the third-order susceptibility $\chi^{(3)}$ exists in any medium [6]. The second-order susceptibility $\chi^{(2)}$ may be used for the second harmonic generation (SHG), sum, and difference frequency generation; the ultrafast Kerr-type third-order susceptibility $\chi^{(3)}$ results in such effects as four-wave mixing (FWM), self-phase modulation (SPM), cross-phase modulation (XPM), third harmonic generation (THG), bistability, and different types of the stimulated light scattering (SLS) [1–6]. Optical-electrical-optical conversion processes can be replaced with the optical signal processing characterized by the femtosecond response time of nonlinearities in optical materials [2, 3]. All-optical signal processing, ultrafast switching, optical generation of ultrashort pulses, the control over the laser radiation frequency spectrum,

wavelength exchange, coherent detection, multiplexing/demultiplexing, and tunable optical delays can be realized by using the nonlinear optical effects [1–4]. However, optical nonlinearities are weak and usually occur only with high-intensity laser beams [1, 6]. An effective nonlinear optical response can be substantially increased by using the plasmonic effects caused by the coherent oscillations of conduction electrons near the surface of noble metal structures [1]. In the case of the extended metal surfaces, the surface plasmon polaritons (SPPs) may occur [1, 7, 8]. SPPs are electromagnetic excitations propagating at the interface between a dielectric and a conductor, evanescently confined in the perpendicular direction [1, 7]. The SPP electromagnetic field decays exponentially on both sides of the interface which results in the subwavelength confinement near the metal surface [1]. The SPP propagation length is limited by the ohmic losses in metal [1, 7, 8].

Nonlinear optical effects can be enhanced by plasmonic excitations as follows: (i) the coupling of light to surface plasmons results in strong local electromagnetic fields; (ii) typically, plasmonic excitations are highly sensitive to dielectric properties of the metal and surrounding medium [1]. In nonlinear optical phenomena, such a sensitivity can be used for the light-induced nonlinear change in the dielectric properties of one of the materials which result in the varying of the plasmonic resonances and the signal beam propagation conditions [1]. Plasmonic excitations are characterized by timescale of several femtoseconds which permits the ultrafast optical signal processing [1]. The SPP field confinement and enhancement can be changed by modifying the structure of the metal or the dielectric near the interface [1]. For example, plasmonic waveguides can be created [1, 7–9]. Nanoplasmonic waveguides can confine and enhance electric fields near the nanometallic surfaces due to the propagating SPPs [9]. Nanoplasmonic waveguide consists of one or two metal films combined with one or two dielectric slabs [9]. Typically, two types of the plasmonic waveguides exist: (i) an insulator/metal/insulator (IMI) heterostructure where a thin metallic layer is placed between two infinitely thick dielectric claddings and (ii) a metal/insulator/metal (MIM) heterostructure where a thin dielectric layer is sandwiched between two metallic claddings [7]. The MIM waveguides for nonlinear optical applications require highly nonlinear dielectrics [9]. The nonlinear metamaterials can significantly increase the nonlinearity magnitude [10]. Investigation of nonlinear metamaterials is related in particular to nonlinear plasmonics and active media [10]. One of the metamaterial nonlinearity mechanisms is based on liquid crystals (LCs) [10]. Tunability and a strongly nonlinear response of metamaterials can be obtained by their integration with LCs offering a practical solution for controlling metamaterial devices [11].

The integration of LCs with plasmonic and metamaterials may be promising for applications in modern photonics due to the extremely large optical nonlinearity of LCs, strong localized electric fields of surface plasmon polaritons (SPPs), and high operation rates as compared to conventional electro-optic devices [12]. Practically all nonlinear optical processes such as wave mixing, self-focusing, self-guiding, optical bistabilities and instabilities, phase conjugation, SLS, optical limiting, interface switching, beam combining, and self-starting laser oscillations have been observed in LCs [13]. LC can be incorporated into nano- and microstructures such as a MIM plasmonic waveguide. Nematic LCs (NLCs) characterized by the orientation long-range order of the elongated molecules are mainly used in optical applications including plasmonics and nanophotonics [11–14]. For instance, light-induced control of fishnet metamaterials infiltrated with NLCs was demonstrated experimentally where a metal-dielectric (Au-MgF_2) sandwich nanostructure on a glass substrate with the inserted NLC was used [11]. However, the NLC applications are limited by their large losses and relatively slow response [14, 15]. The light scattering in smectic A LC (SmALC) waveguides had been studied theoretically and

experimentally, and it was shown that the scattering losses in SmALC are much lower than in NLC due to a higher degree of the long-range order [15]. SmALC can be useful in nonlinear optical applications and low-loss active waveguide devices for integrated optics [14, 15].

SmALCs are characterized by a positional long-range order in the direction of the elongated molecular axis and demonstrate a layer structure with a layer thickness $d_{SmA} \approx 2nm$ [14]. Inside a smectic layer, the molecules form a two-dimensional liquid [14]. Actually, SmALC can be considered as a natural nanostructure. The structures of NLC with the elongated molecules directed mainly along the vector director $\vec{n}$ and the homeotropically oriented SmALC with the layer plane parallel to the claddings are shown in **Figure 1a** and **b**, respectively.

The nonlinear optical phenomena in SmALC such as a light self-focusing, self-trapping, SPM, SLS, and FWM based on the specific mechanism of the third-order optical nonlinearity related to the smectic layer normal displacement had been investigated theoretically [16–28]. In particular it has been shown that at the interface of a metal and SmALC, the counter-propagating SPPs created the dynamic grating of the smectic layer normal displacement $u(x,z,t)$, and the SLS of the interfering SPPs occurred [22, 23, 26]. We also investigated the behavior of SPP mode in a MIM waveguide with the SmALC core [24, 26]. In such a waveguide, SPP behaves as a strongly localized transverse magnetic (TM) mode which creates the localized smectic layer normal deformation and undergoes SPM [24, 26].

In this chapter we consider theoretically the interaction of the counter-propagating SPP modes in the MIM waveguide with the SmALC core. The interfering SPP TM modes with the close optical frequencies $\omega_{1,2}$ create a localized dynamic grating of the smectic layer normal displacement $u(x,z,t)$ with the frequency $\Delta\omega = \omega_1 - \omega_2 \ll \omega_1$ which results in the nonlinear polarization and stimulated scattering of SPPs. We solved simultaneously the equation of motion for smectic layers in the electric field of the interfering SPP modes and the Maxwell equations for the SPPs in the MIM waveguide taking into account the nonlinear polarization. We used the slowly varying amplitude (SVA) approximation for the SPPs [6]. We evaluated the magnitudes and phases of the coupled SPP SVAs. It is shown that the energy exchange between the coupled SPPs and XPM takes place. We also evaluated the SPP-induced smectic layer displacement and SmALC hydrodynamic velocity. We have shown that the high-frequency localized electric field can occur in the MIM waveguide with the SmALC core due to the flexoelectric effect [28].

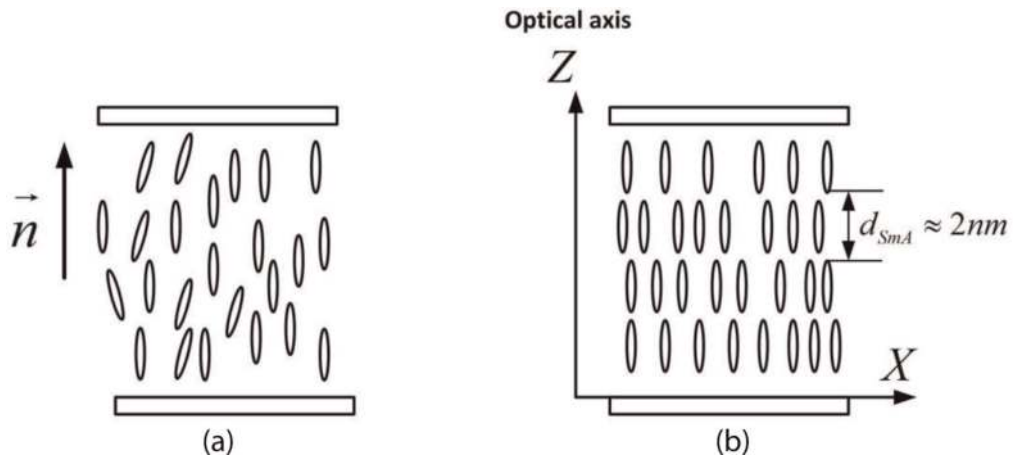

Figure 1.
The structure of molecular alignment of a nematic liquid crystal (NLC) (a) and the homeotropically oriented smectic A liquid crystal (SmALC). The molecules are perpendicular to the layer plane (b).

The chapter is constructed as follows. The hydrodynamics of SmALC in the external electric field is considered in Section 2. The SPP modes of the MIM waveguide are derived in Section 3. The SPP SVAs, the smectic layer dynamic grating amplitude, and the SmALC hydrodynamic velocity are evaluated in Section 4. The conclusions are presented in Section 5.

2. Hydrodynamics of SmALC in the external electric field

In this section we briefly discuss the SmALC hydrodynamics and derive the equation of motion for the smectic layer normal displacement $u(x,y,z,t)$ in the external electric field $\vec{E}(x,y,z,t)$. SmALC can be described by the one-dimensional periodic density wave due to its layered structure.

Smectic layer oscillations $u(x,y,z,t)$ in the external electric field $\vec{E}(x,y,z,t)$ are shown in **Figure 2**. Hydrodynamics of SmALC in general case is very complicated because SmALC is a strongly anisotropic viscous liquid including the layer oscillations, the mass density, and the elongated molecule orientation variations [29–31]. However, the elastic constant related to the SmALC bulk compression is much larger than the elastic constant $B \approx 10^6 - 10^7 \mathrm{J\ m^{-3}}$ related to the smectic layer compression [29–31]. The layers can oscillate without the change of the mass density [29–31]. For this reason two uncoupled acoustic modes can propagate in SmALC: the ordinary longitudinal sound wave caused by the mass density variation and the second-sound (SS) wave caused by the layer oscillations [29–31]. SS wave is characterized by strongly anisotropic dispersion relation being neither purely transverse nor longitudinal. It propagates in the direction oblique to the layer plane

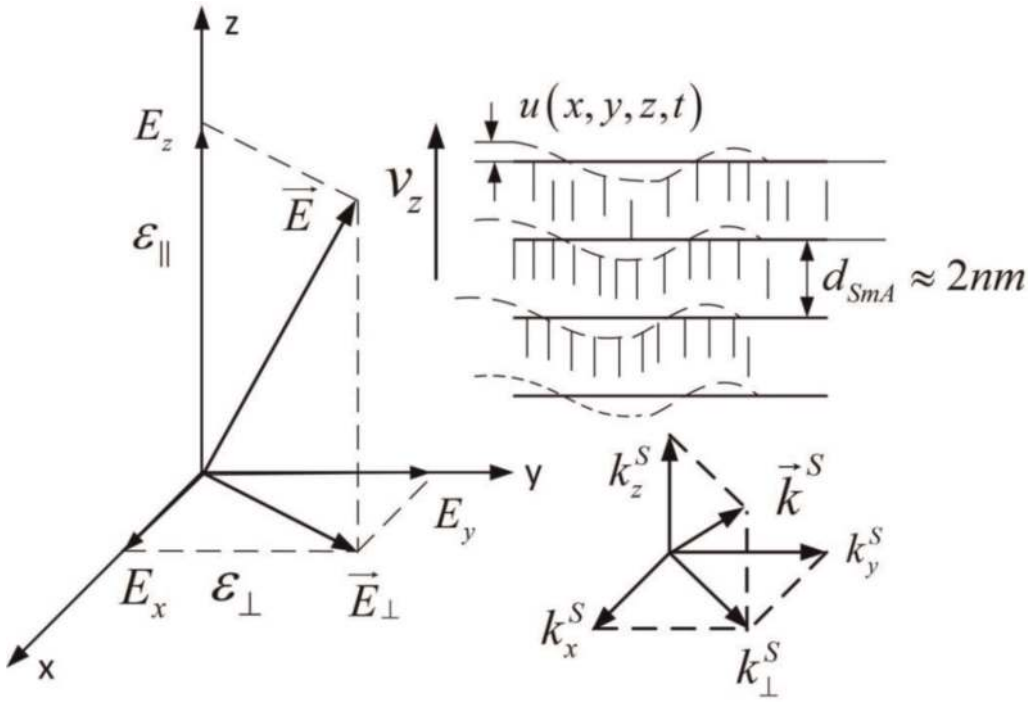

Figure 2.

The SmALC layer oscillations $u(x,y,z,t)$ in the external electric field $\vec{E}(x,y,z,t)$. $\vec{k}^S$ is the second-sound (SS) wave vector, v_z is the hydrodynamic velocity perpendicular to the layer plane; $\varepsilon_{\|}$ and $\varepsilon_{\perp}$ are the diagonal components of the permittivity tensor parallel and perpendicular to the optical axis, respectively.

and vanishes for the wave vector $\vec{k}^S$ perpendicular or parallel to the layer plane [29]. SmALC is characterized by the complex order parameter, and SS represents the oscillations of the order parameter phase [29]. SS in SmALC has been observed experimentally by different methods [32–34]. The system of hydrodynamic equations for the incompressible SmALC under the constant temperature far from the phase transition has the form [29–31]

$$div\ \vec{v} = 0 \tag{1}$$

$$\rho\frac{\partial v_i}{\partial t} = -\frac{\partial \Pi}{\partial x_i} + \Lambda_i + \frac{\partial \sigma'_{ik}}{\partial x_k} \tag{2}$$

$$\Lambda_i = -\frac{\delta F}{\delta u_i} \tag{3}$$

$$\sigma'_{ik} = \alpha_0\delta_{ik}A_{ll} + \alpha_1\delta_{iz}A_{zz} + \alpha_4 A_{ik} + \alpha_{56}(\delta_{iz}A_{zk} + \delta_{kz}A_{zi}) + \alpha_7\delta_{iz}\delta_{kz}A_{ll} \tag{4}$$

$$A_{ik} = \frac{1}{2}\left(\frac{\partial v_i}{\partial x_k} + \frac{\partial v_k}{\partial x_i}\right) \tag{5}$$

$$v_z = \frac{\partial u}{\partial t} \tag{6}$$

Here, $\vec{v}$ is the hydrodynamic velocity, $\rho \approx 10^3 \mathrm{kg\,m^{-3}}$ is the SmALC mass density, Π is the pressure, $\vec{\Lambda}$ is the generalized force density, σ'_{ik} is the viscous stress tensor, $\alpha_i \approx 10^{-1}\mathrm{kg(s\,m)^{-1}}$ are the viscosity Leslie coefficients, $\delta_{ik} = 1, i = k; \delta_{ik} = 0, i \neq k$, and F is the free energy density of SmALC. Typically, SmALC is supposed to be an incompressible liquid according to Equation (1) [29]. For this reason, we assume that the pressure $\Pi = 0$ and the SmALC free energy density F do not depend on the bulk compression [29–31]. We are interested in the SS propagation and neglect the ordinary sound mode. The normal layer displacement $u(x, y, z, t)$ by definition has only one component along the Z axis. In such a case, the generalized force density has only the Z component according to Eq. (3): $\vec{\Lambda} = (0, 0, \Lambda_z)$. Eq. (6) is specific for SmALC since it determines the condition of the smectic layer continuity [29–31]. The SmALC free energy density F in the presence of the external electric field $\vec{E}(x, y, z, t)$ has the form [29–31]

$$F = \frac{1}{2}B\left(\frac{\partial u}{\partial z}\right)^2 + \frac{1}{2}K\left(\frac{\partial^2 u}{\partial x^2} + \frac{\partial^2 u}{\partial y^2}\right)^2 - \frac{1}{2}\varepsilon_0\varepsilon_{ik}E_iE_k \tag{7}$$

Here $K \sim 10^{-11}N$ is the Frank elastic constant associated with the SmALC orientational energy inside layers, ε_0 is the free space permittivity, and ε_{ik} is the SmALC permittivity tensor including the terms defined by the smectic layer strains. The purely orientational second term in the free energy density F (7) can be neglected since for the typical values of the elastic constants B and $K\ K\left(k_\perp^S\right)^2 \ll B$ where $k_\perp^S$, the SS wave vector component is parallel to the layer plane. The permittivity tensor ε_{ik} is given by [30]

$$\begin{aligned} &\varepsilon_{xx} = \varepsilon_{yy} = \varepsilon_\perp + a_\perp\frac{\partial u}{\partial z}; \varepsilon_{zz} = \varepsilon_\parallel + a_\parallel\frac{\partial u}{\partial z}; \\ &\varepsilon_{xz} = \varepsilon_{zx} = -\varepsilon_a\frac{\partial u}{\partial x}; \varepsilon_{yz} = \varepsilon_{zy} = -\varepsilon_a\frac{\partial u}{\partial y}; \varepsilon_a = \varepsilon_\parallel - \varepsilon_\perp \end{aligned} \tag{8}$$

where $\varepsilon_{\parallel}, \varepsilon_{\perp}$ are the diagonal components of the permittivity tensor ε_{ik} along and perpendicular to the optical axis and $a_{\perp} \sim 1, a_{\parallel} \sim 1$ are the phenomenological dimensionless coefficients [29, 30]. SmALC is an optically uniaxial medium with the optical Z axis perpendicular to the smectic layer plane [29–31]. Combining Eqs. (1)–(8), we obtain the equation of motion for the smectic layer normal displacement $u(x,y,z,t)$ in the electric field $\vec{E}(x,y,z,t)$ [16, 17]:

$$\begin{aligned} &-\rho\nabla^2\frac{\partial^2 u}{\partial t^2}+\left[\alpha_1\nabla_{\perp}^2\frac{\partial^2}{\partial z^2}+\frac{1}{2}(\alpha_4+\alpha_{56})\nabla^2\nabla^2\right]\frac{\partial u}{\partial t}+B\nabla_{\perp}^2\frac{\partial^2 u}{\partial z^2} \\ &=\frac{\varepsilon_0}{2}\nabla_{\perp}^2\left[\frac{\partial}{\partial z}\left(a_{\perp}\left(E_x^2+E_y^2\right)+a_{\parallel}E_z^2\right)-2\varepsilon_a\left(\frac{\partial}{\partial x}\left(E_xE_z\right)+\frac{\partial}{\partial y}\left(E_yE_z\right)\right)\right] \end{aligned} \tag{9}$$

Here $\nabla_{\perp}^2 u = \partial^2 u/\partial x^2 + \partial^2 u/\partial y^2$. In the absence of the external electric field, the homogeneous solution of the equation of motion (9) represents the SS wave with the dispersion relation [29]:

$$\Omega_S = s_0\frac{k_{\perp}^S k_z^S}{k^S}; s_0 = \sqrt{\frac{B}{\rho}} \tag{10}$$

Here, $\left(k_{\perp}^S\right)^2 = \left(k_x^S\right)^2 + \left(k_y^S\right)^2$ and Ω_S and s_0 are the SS frequency and velocity, respectively [29]. It is seen from Eq. (10) that the SS frequency $\Omega_S = 0$ for the propagation direction along the smectic layer plane and perpendicular to it. The decay constant Γ is given by

$$\Gamma = \frac{1}{2\rho}\left[\alpha_1\frac{\left(k_{\perp}^S\right)^2\left(k_z^S\right)^2}{\left(k^S\right)^2}+\frac{1}{2}(\alpha_4+\alpha_{56})\left(k^S\right)^2\right] \tag{11}$$

If the viscosity terms responsible for the SS wave decay can be neglected, then the homogeneous part of Eq. (9) reduces to the SS wave equation with the dispersion relation (10) [29–31]:

$$\rho\nabla^2\frac{\partial^2 u}{\partial t^2} = B\nabla_{\perp}^2\frac{\partial^2 u}{\partial z^2}$$

We use equation of motion (9) for the evaluation of the light-enhanced dynamic grating $u(x,y,z,t)$.

3. SPP modes in a MIM waveguide with SmALC core

LC slab optical waveguide represents a LC layer of a thickness about 1 μm confined between two glass slides of lower refractive index than LC [14]. LC as a waveguide core provides the photonic signal modulation and switching by using the electro-optic or nonlinear optical effects of LC mesophases [35]. For instance, the large optical nonlinearities were implemented in order to create optical paths by photonic control of solitons in NLC [35]. Various electrode geometries may create due to the electro-optic effect periodically modulated LC core waveguides which can serve as efficient guided distributed Bragg reflectors with the tuning ranges of about 100–1550 nm optical wavelength range [35]. Plasmonic waveguides based on

the manipulation and routing of SPPs can demonstrate a subwavelength beyond the diffraction limit together with large bandwidth and high operation rate typical for photonics [36]. The plasmonic devices can be integrated into nanophotonic chips due to their small scale and the compatibility with the VLSI electronic technology [36]. Plasmonic devices are the promising candidates for future integrated photonic circuits for broadband light routing, switching, and interconnecting [36]. It has been shown that different plasmonic structures can provide SPP light waveguiding determining the SPP mode properties [36]. MIM waveguide representing a dielectric sandwiched between two metal slabs attracted a research interest as a basic component of nanoscale plasmonic integrated circuits [37]. LC-tunable waveguides have been proposed as a core element of low-power variable attenuators, phase-shifters, switches, filters, tunable lenses, beam steers, and modulators [37, 38]. Typically NLCs have been used due to their strong optical anisotropy, responsivity to external electric and magnetic fields, and low power [37, 38]. Different types of NLC plasmonic waveguides have been proposed and investigated theoretically [36–38]. Recently, SmALCs attracted attention due to their layered structure and reconfigurable layer curvature [39]. The possibility of the dynamic variation of smectic layer configuration by external fields is intensively studied [39]. We investigated theoretically SLS in the optical slab waveguide with the SmALC core where the third-order optical nonlinearity mechanism was related to the smectic layer dynamic grating created by the interfering waveguide modes [27]. We also considered theoretically the MIM waveguide with the SmALC core [24, 26].

The structure of such a symmetric waveguide of the thickness 2d is shown in **Figure 3** [24, 26]. The plane of the waveguide is perpendicular to the SmALC optical axis Z. The SmALC in the waveguide core is homeotropically oriented, i.e., the smectic layers are parallel to the waveguide claddings $z = \pm d$, while the SmALC elongated molecules are mainly parallel to the Z axis [29]. Typically the waveguide dimension in the Y axis direction is much larger than d, and the dependence on the coordinate y in Eqs. (8) and (9) can be omitted. Than we obtain $u = u(x, z, t)$, $\nabla^2 u = \partial^2 u/\partial x^2 + \partial^2 u/\partial z^2$, $\nabla_\perp^2 u = \partial^2 u/\partial x^2$, $\left(k_\perp^S\right)^2 = \left(k_x^S\right)^2$, and the SmALC permittivity tensor (8) takes the form

$$\varepsilon_{xx} = \varepsilon_\perp + a_\perp \frac{\partial u}{\partial z};\ \varepsilon_{zz} = \varepsilon_\parallel + a_\parallel \frac{\partial u}{\partial z};\ \varepsilon_{xz} = \varepsilon_{zx} = -\varepsilon_a \frac{\partial u}{\partial x};\varepsilon_a = \varepsilon_\parallel - \varepsilon_\perp \qquad (12)$$

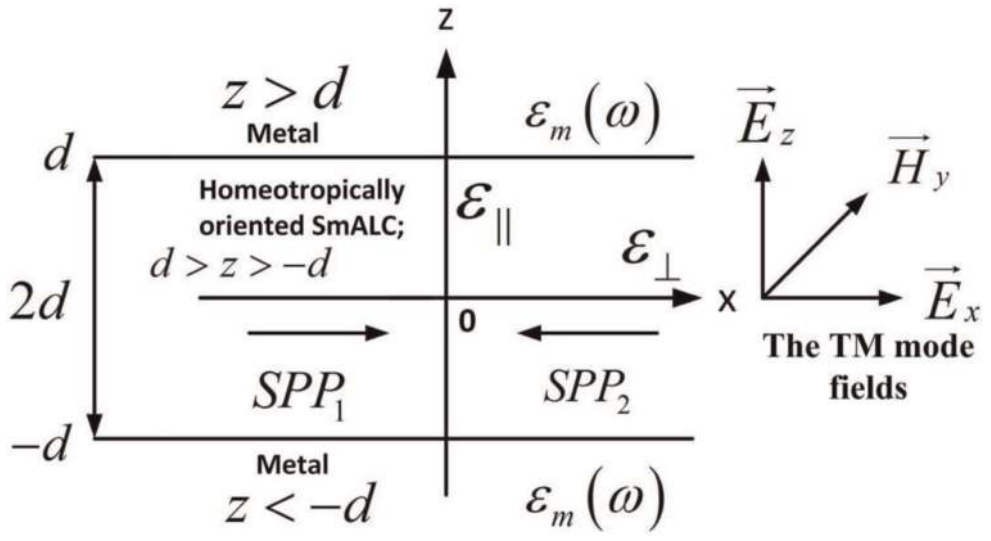

Figure 3.
The MIM waveguide with the homeotropically oriented SmALC core and counter-propagating SPPs.

The permittivity $\varepsilon_m(\omega)$ of the metal claddings is described by the Drude model [7, 8]:

$$\varepsilon_m(\omega) = 1 - \frac{\omega_p^2}{[\omega^2 + (i\omega/\tau)]} \tag{13}$$

where $\omega_p = \sqrt{n_0 e^2/(\varepsilon_0 m)}$ is the plasma frequency of the free electron gas; n_0 is the free electron density in the metal;e, m are the electron charge and mass, respectively; and ω, τ are the SPP angular frequency and lifetime, respectively [7, 8]. The electric field $\vec{E}(x,z,t)$ of the optical wave propagating in a nonlinear medium is described by the following wave equation including the nonlinear part of the electric induction $\vec{D}^{NL}$ [6]:

$$curlcurl\vec{E} + \mu_0 \frac{\partial^2 \vec{D}^{L}}{\partial t^2} = -\mu_0 \frac{\partial^2 \vec{D}^{NL}}{\partial t^2} \tag{14}$$

Here μ_0 is the free space permeability and $\vec{D}^{L}$ is the nonlinear part of the electric induction. The SPP can propagate in the plasmonic waveguide only as a transverse magnetic (TM) mode with the electric and magnetic fields given by $\vec{E}_{TM} = (E_x, 0, E_z)$; $\vec{H}_{TM} = \left(0, H_y, 0\right)$ [7]. In such a case, we obtain for $\vec{D}^{L}$ and $\vec{D}^{NL}$ in SmALC using Eq. (12)

$$D_x^L = \varepsilon_0 \varepsilon_\perp E_x;\ D_z^L = \varepsilon_0 \varepsilon_\parallel E_z \tag{15}$$

$$D_x^{NL} = \varepsilon_0 \left(a_\perp \frac{\partial u}{\partial z} E_x - \varepsilon_a \frac{\partial u}{\partial x} E_z \right);\ D_z^{NL} = \varepsilon_0 \left(a_\parallel \frac{\partial u}{\partial z} E_z - \varepsilon_a \frac{\partial u}{\partial x} E_x \right) \tag{16}$$

The linear part $\vec{D}_m^{L}$ of the electric induction in the metal claddings has the form: $\vec{D}_m^{L} = \varepsilon_0 \varepsilon_m(\omega)\vec{E}$ [7]. The SPP TM mode electric and magnetic fields for $|z| > d$ in the metal claddings $\vec{H}_{1,2}(x,z,t)$, $\vec{E}_{1,2}(x,z,t)$ and for $|z| \le d$ in SmALC $\vec{H}_{SA}(x,z,t)$, $\vec{E}_{SA}(x,z,t)$ have the form [24, 26]

$$\vec{H}_{1,2}(x,z,t) = \frac{1}{2}\vec{a}_y H_{1,20} \exp\left(\mp k_z^m z + ik_x x - i\omega t \right) + c.c.,\ |z| > d \tag{17}$$

$$\vec{E}_{1,2}(x,z,t) = \frac{1}{2}\left[\vec{a}_x E_{1,2x0} + \vec{a}_z E_{1,2z0} \right] \exp\left(\mp k_z^m z + ik_x x - i\omega t \right) + c.c.,\ |z| > d \tag{18}$$

$$\vec{H}_{SA}(x,z,t) = \frac{1}{2}\vec{a}_y \left[A \exp\left(k_z^S z \right) + B \exp\left(-k_z^S z \right) \right] \exp\left(ik_x x - i\omega t \right) + c.c.,\ |z| \le d \tag{19}$$

$$\begin{aligned} \vec{E}_{SA}(x,z,t) = \frac{1}{2}\{ & \vec{a}_x \frac{k_z^S}{i\omega\varepsilon_0\varepsilon_\perp} \left[A \exp\left(k_z^S z \right) - B \exp\left(-k_z^S z \right) \right] \\ & - \vec{a}_z \frac{k_x}{\omega\varepsilon_0\varepsilon_\parallel} \left[A \exp\left(k_z^S z \right) + B \exp\left(-k_z^S z \right) \right] \} \exp i(k_x x - \omega t) + c.c.;\ |z| \le d \end{aligned} \tag{20}$$

Here c.c. stands for complex conjugate. The SPP fields (17)–(20) are confined in the Z direction. In the linear approximation substituting expressions (15), (18), and

(20) into the homogeneous part of the wave equation (14) for the claddings and SmALC core, respectively, we obtain the following expressions for the complex wave numbers k_z^m and k_z^S [24, 26]:

$$k_z^m = \sqrt{k_x^2 - \varepsilon_m(\omega)\omega^2/c^2} \tag{21}$$

$$k_z^S = \sqrt{k_x^2(\varepsilon_\perp/\varepsilon_\parallel) - \omega^2\varepsilon_\perp/c^2} \tag{22}$$

where c is the free space light velocity. The boundary conditions for the fields (17)–(20) at the interfaces $z = \pm d$ have the form [7, 8]

$$H_{1y}(z = d) = H_{SAy}(z = d);\ H_{2y}(z = -d) = H_{SAy}(z = -d) \tag{23}$$

$$E_{1x}(z = d) = E_{SAx}(z = d);\ E_{2x}(z = -d) = E_{SAx}(z = -d) \tag{24}$$

Substituting expressions (17)–(20) into Eqs. (23) and (24), we obtain the dispersion relation for the SPP TM modes in the MIM waveguide given by [24, 26]

$$\exp\left(-4k_z^S d\right) = \left(\frac{k_z^m}{\varepsilon_m(\omega)} + \frac{k_z^S}{\varepsilon_\perp}\right)^2 \left(\frac{k_z^m}{\varepsilon_m(\omega)} - \frac{k_z^S}{\varepsilon_\perp}\right)^{-2} \tag{25}$$

Dispersion relation obtained for the general case of different claddings [7] coincides with expression (25) for the symmetric structure with the same claddings. The results of the numerical solution of Eq. (25) for the typical values of the MIM waveguide parameters and the SPP frequencies ω corresponding to the optical wavelength range $\lambda_{opt} \sim 1 - 1.6$ μm and $2d \sim 1$ μm are presented in **Figures 4** and **5**.

These results show that $\mathrm{Re}\,k_z^S \sim 10^6 m^{-1} \gg \mathrm{Im}k_z^S \sim 10^4 m^{-1}$ and $\mathrm{Re}\,k_x \sim 10^7 m^{-1} \gg \mathrm{Im}k_x \sim 10^3 m^{-1}$ [24, 26]. In such a case, the SPP oscillation length in the Z direction is defined by the relationship $2\pi\left(\mathrm{Im}k_z^S\right)^{-1} \sim 10^{-4} m \gg d \sim 10^{-6} m$, and $\mathrm{Im}k_z^S$ can be neglected inside the MIM waveguide, and $k_z^S \approx \mathrm{Re}\,k_z^S$ [24, 26]. The SPP propagation length in the X direction $L_{SPP} = (\mathrm{Im}k_x)^{-1} \sim 10^{-4} - 10^{-3} m \gg \lambda_{SPP} = 2\pi(\mathrm{Re}\,k_x)^{-1} < 10^{-6} m$ where λ_{SPP} is the SPP wavelength. Hence, at the optical wavelength-scale distances, $\mathrm{Im}k_x$ can be neglected, and $k_x \approx \mathrm{Re}\,k_x$ [24, 26].

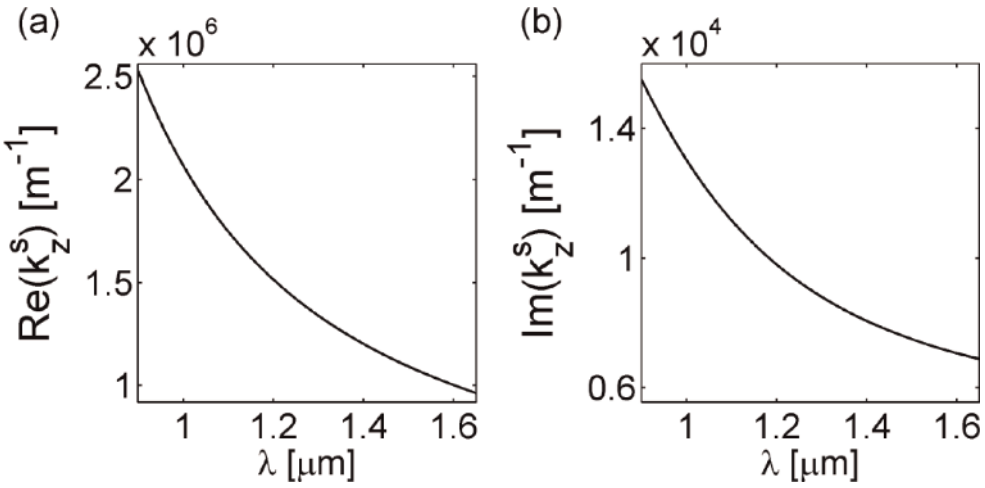

Figure 4.
The spectral dependence of $\mathrm{Re}\,k_z^S$(a) and $\mathrm{Im}k_z^S$ (b).

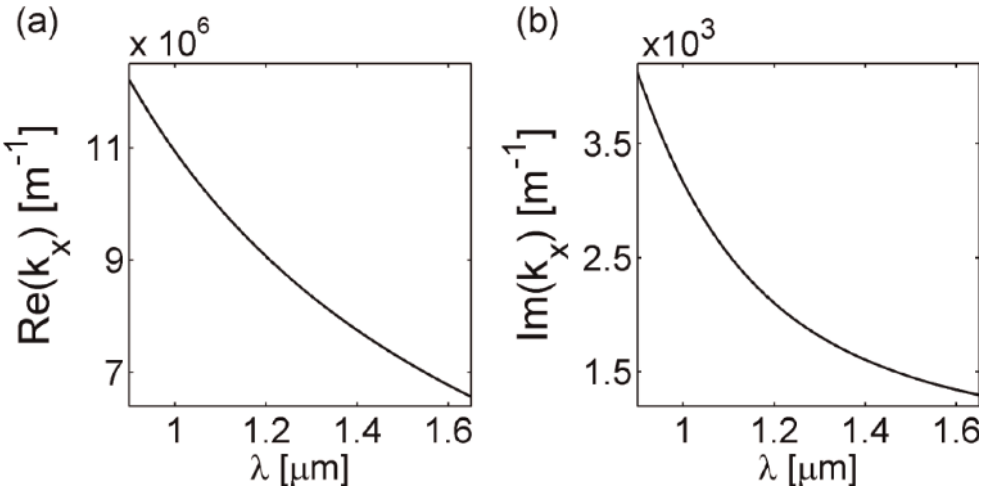

Figure 5.
The spectral dependence of Re k_x (a) and Imk_x (b).

Consequently, for a given optical frequency ω, a single localized TM mode can exist in the SmALC core of the MIM waveguide with the electric field $\vec{E}_{SA}(x,z,t)$ given by [24, 26]

$$\vec{E}_{SA} = E_0\left[\vec{a}_x \cosh\left(\left(\mathrm{Re}\,k_z^S\right)z\right) - \vec{a}_z i\frac{k_x\varepsilon_\perp}{k_z^S\varepsilon_\parallel}\sinh\left(\left(\mathrm{Re}\,k_z^S\right)z\right)\right] \times \exp\left[i((\mathrm{Re}\,k_x)x - \omega t)\right] + c.c. \tag{26}$$

The numerical estimations show that for the SPP modes with the close optical frequencies $\omega_{1,2} \sim 10^{15}\mathrm{s}^{-1}$ and the frequency difference $\Delta\omega = \omega_1 - \omega_2 \sim 10^8 s^{-1} \ll \omega_1$, the wave numbers of the both SPPs $k_{z1,2}^S$ and $k_{x1,2}$ are practically equal. As a result, only counter-propagating SPP modes can strongly interact in the MIM core creating the dynamic grating of smectic layers as it is seen from Eq. (9). The electric field of the counter-propagating SPP modes of the type (26) in the MIM waveguide SmALC core has the form

$$\vec{E}_{SA1,2} = E_{SA1,20}\left[\vec{a}_x \cosh\left(\left(\mathrm{Re}\,k_z^S\right)z\right) \mp \vec{a}_z i\frac{k_x\varepsilon_\perp}{k_z^S\varepsilon_\parallel}\sinh\left(\left(\mathrm{Re}\,k_z^S\right)z\right)\right] \times \exp\left[\pm i(\mathrm{Re}\,k_x)x - i\omega_{1,2}t\right] + c.c. \tag{27}$$

Substituting expression (27) into equation of motion (9), we obtain the expression of the smectic layer displacement localized dynamic grating $u(x,z,t)$:

$$u(x,z,t) = U_0 \sinh\left(2\left(\mathrm{Re}\,k_z^S\right)z\right)\exp\left[i(2(\mathrm{Re}\,k_x)x - \Delta\omega t)\right] + c.c. \tag{28}$$

Here

$$U_0 = -\frac{4\varepsilon_0 E_{SA10}E_{SA20}^*}{G\left(k_x, k_z^S, \Delta\omega\right)}(\mathrm{Re}\,k_x)^2\left(\mathrm{Re}\,k_z^S\right)h;$$
$$h = \left\{a_\perp - a_\parallel\frac{|k_x|^2\varepsilon_\perp^2}{\left|k_z^S\right|^2\varepsilon_\parallel^2} - 2\varepsilon_a\frac{(\mathrm{Re}\,k_x)^2\varepsilon_\perp}{\left(\mathrm{Re}\,k_z^S\right)^2\varepsilon_\parallel}\right\} \tag{29}$$

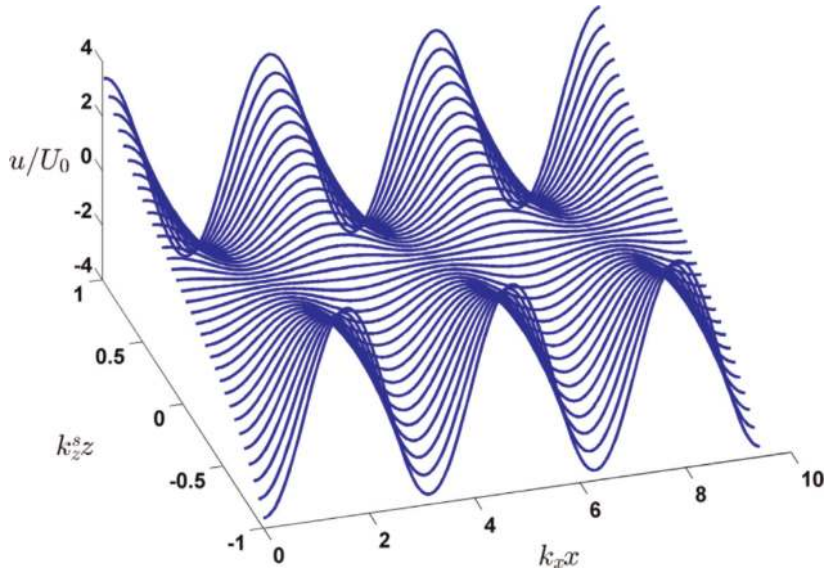

Figure 6.
The normalized smectic layer displacement $u(x,z,t=t_0)$ for the optical wavelength $\lambda_{opt} = 1.6\ \mu m$.

$$G\left(k_x, k_z^S, \Delta\omega\right) = 4\rho(\Delta\omega)^2\left[-(\operatorname{Re}k_x)^2 + \left(\operatorname{Re}k_z^S\right)^2\right]$$
$$-i\Delta\omega\{-\alpha_1(2\operatorname{Re}k_x)^2\left(2\operatorname{Re}k_z^S\right)^2 \tag{30}$$
$$+\frac{1}{2}(\alpha_4+\alpha_{56})\left[-(2\operatorname{Re}k_x)^2 + \left(2\operatorname{Re}k_z^S\right)^2\right]^2\} - B(2\operatorname{Re}k_x)^2\left(2\operatorname{Re}k_z^S\right)^2$$

Expression (28) is the enhanced solution of Eq. (9). The homogeneous solution of Eq. (9) is overdamped for the typical values of SmALC parameters and $\Delta\omega \sim 10^8 s^{-1}$, and it can be neglected. The normalized smectic layer displacement $u(x,z,t=t_0)/U_0$ for the optical wavelength $\lambda_{opt} = 1.6\mu m$ is shown in **Figure 6**. It is seen from **Figure 6** that the dynamic grating is localized inside the MIM waveguide in the Z direction and oscillates in the propagation direction X.

4. Nonlinear interaction of SPPs in the MIM waveguide

The light-enhanced dynamic grating (28) results in the nonlinear polarization defined by Eq. (16). In order to investigate the interaction of the counter-propagating SPPs (27), we should solve wave Eq. (14) including the nonlinear term $\vec{D}^{NL}$. We use the SVA approximation for the SPP electric field amplitudes $E_{SA1,20}(t) = |E_{SA1,20}(t)|\exp i\theta_{SA1,2}(t)$ where $|E_{SA1,20}(t)|$ and $\theta_{SA1,2}(t)$ are the SVA magnitudes and phases, respectively [6]. For the distances of the order of magnitude of the SPP wavelength $\lambda_{SPP} < 1\ \mu m$, the dependence of SAVs on the x coordinate can be neglected. We assume according to the SVA approximation that

$$\left|\frac{\partial^2 E_{SA1,20}}{\partial t^2}\right| \ll \omega_1\left|\frac{\partial E_{SA1,20}}{\partial t}\right| \tag{31}$$

Substituting expressions (27) and (28) into Eqs. (16), we evaluate the nonlinear part $\vec{D}^{NL}$ of the electric induction in SmALC. Then, substituting relationships (15),

(16), and (27) into wave equation (14), taking into account the dispersion relation (22), neglecting the terms $\partial^2 E_{SA1,20}/\partial t^2$ according to condition (31), combining the phase-matched terms with the frequencies $\omega_{1,2}$, and dividing the real and imaginary parts, we derive the equations for the SVA magnitudes $|E_{SA1,20}(t)|$ and phases $\theta_{SA1,2}(t)$. They have the form

$$\begin{aligned}&\frac{1}{\omega_{1,2}}\frac{\partial|E_{SA1,20}(t)|^2}{\partial t}F_1(z)\\&=\mp\frac{8\varepsilon_0\mathrm{Im}G\left(k_x,k_z^S,\Delta\omega\right)[\,\mathrm{Re}\,k_x]^2h|E_{SA10}(t)|^2|E_{SA20}(t)|^2}{\varepsilon_\perp\left|G\left(k_x,k_z^S,\Delta\omega\right)\right|^2}F_2(z)\end{aligned}\tag{32}$$

$$\begin{aligned}&\frac{1}{\omega_{1,2}}\frac{\partial\theta_{1,2}}{\partial t}F_1(z)\\&=-\frac{4\varepsilon_0\,\mathrm{Re}\,G\left(k_x,k_z^S,\Delta\omega\right)|E_{SA2,10}(t)|^2[\,\mathrm{Re}\,k_x]^2h}{\varepsilon_\perp\left|G\left(k_x,k_z^S,\Delta\omega\right)\right|^2}F_2(z)\end{aligned}\tag{33}$$

Here we assumed that the factor $\exp[\pm(\mathrm{Im}k_x)x]\approx 1$ for the distances $x\ll(\mathrm{Im}k_x)^{-1}$. The functions $F_{1,2}(z)$ describing the SPP mode localization inside the MIM waveguide are given by

$$F_1(z)=\cosh^2\left(k_z^Sz\right)+\frac{|k_x|^2}{\left|k_z^S\right|^2}\sinh^2\left(k_z^Sz\right)\tag{34}$$

$$\begin{aligned}F_2(z)=\;&\cosh^2\left(k_z^Sz\right)\left[\cosh\left(2k_z^Sz\right)\left(a_\perp\left(k_z^S\right)^2+\varepsilon_a\frac{\varepsilon_\perp}{\varepsilon_\parallel}k_x^2\right)-\varepsilon_a\frac{\varepsilon_\perp}{\varepsilon_\parallel}k_x^2\right]\\&-k_x^2\sinh^2\left(k_z^Sz\right)\left[\cosh\left(2k_z^Sz\right)\left(a_\parallel\frac{\varepsilon_\perp}{\varepsilon_\parallel}-\varepsilon_a\right)-\varepsilon_a\right]\end{aligned}\tag{35}$$

Here we neglected the small quantities $\mathrm{Im}k_x$ and $\mathrm{Im}k_z^S$ assuming that for $x\ll(\mathrm{Im}k_x)^{-1}$ and $|z|\le d$, we may use the relationships $k_x\approx\mathrm{Re}\,k_x$ and $k_z^S\approx\mathrm{Re}\,k_z^S$. We integrate both parts of Eqs. (32) and (33) over the MIM waveguide thickness $-d\le z\le d$ [40]. After the integration, Eqs. (32) and (33) take the form

$$\begin{aligned}&\frac{1}{\omega_{1,2}}\frac{\partial|E_{SA1,20}(t)|^2}{\partial t}\\&=\mp\frac{8\varepsilon_0\mathrm{Im}G\left(k_x,k_z^S,\Delta\omega\right)k_x^2h\left(k_z^S\right)^2}{\varepsilon_\perp\left|G\left(k_x,k_z^S,\Delta\omega\right)\right|^2}\\&\quad\times|E_{SA10}(t)|^2|E_{SA20}(t)|^2F_N\left(k_x,k_z^S\right)\end{aligned}\tag{36}$$

$$\begin{aligned}&\frac{1}{\omega_{1,2}}\frac{\partial\theta_{1,2}}{\partial t}\\&=-\frac{4\varepsilon_0\,\mathrm{Re}\,G\left(k_x,k_z^S,\Delta\omega\right)k_x^2h\left(k_z^S\right)^2}{\varepsilon_\perp\left|G\left(k_x,k_z^S,\Delta\omega\right)\right|^2}|E_{SA2,10}(t)|^2F_N\left(k_x,k_z^S\right)\end{aligned}\tag{37}$$

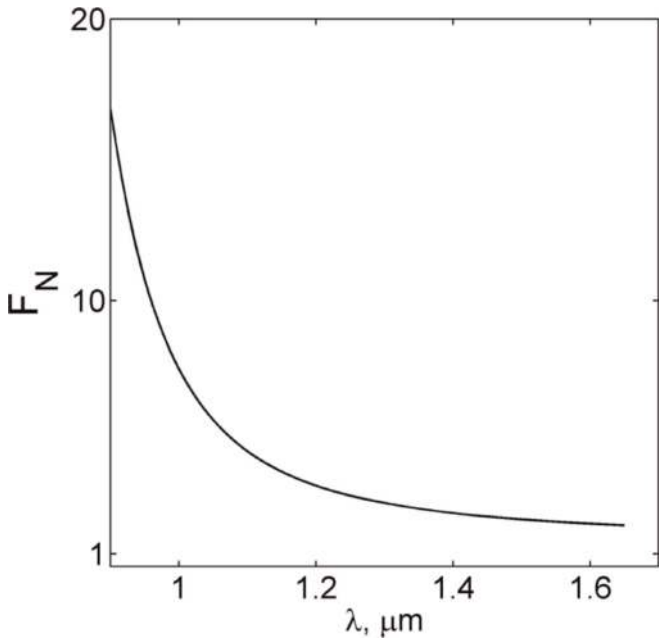

Figure 7.
The spectral dependence of the localization factor $F_N\left(k_x, k_z^S\right)$.

where the localization factor $F_N\left(k_x, k_z^S\right)$ is given by

$$\begin{aligned} & F_N\left(k_x, k_z^S\right) \\ & = \{\frac{\left[\sinh\left(4k_z^S d\right) + 4k_z^S d\right]}{4}\left[a_\perp - a_\parallel \frac{\varepsilon_\perp k_x^2}{\varepsilon_\parallel\left(k_z^S\right)^2} + \varepsilon_a \frac{k_x^2}{\left(k_z^S\right)^2}\left(1 + \frac{\varepsilon_\perp}{\varepsilon_\parallel}\right)\right] \\ & + \sinh\left(2k_z^S d\right)\left(a_\perp + a_\parallel \frac{\varepsilon_\perp k_x^2}{\varepsilon_\parallel\left(k_z^S\right)^2}\right) - \left(2k_z^S d\right)\varepsilon_a \frac{k_x^2}{\left(k_z^S\right)^2}\left(1 + \frac{\varepsilon_\perp}{\varepsilon_\parallel}\right)\} \\ & \times\left[\sinh\left(2k_z^S d\right)\left(1 + \frac{k_x^2}{\left(k_z^S\right)^2}\right) + \left(2k_z^S d\right)\left(1 - \frac{k_x^2}{\left(k_z^S\right)^2}\right)\right]^{-1} \end{aligned} \tag{38}$$

The spectral dependence of the localization factor $F_N\left(k_x, k_z^S\right)$ is presented in **Figure 7**.

It is seen from **Figure 7** that $F_N\left(k_x, k_z^S\right)$ is varying by an order of magnitude in the range of the optical wavelengths essential for optical communications. The addition of Eq. (36) results in the following conservation condition [6]:

$$\frac{\partial}{\partial t}\left(\frac{\left|E_{SA10}(t)\right|^2}{\omega_1} + \frac{\left|E_{SA20}(t)\right|^2}{\omega_2}\right) = 0 \tag{39}$$

We obtain from Eq. (39) the Manley-Rowe relation for the SVA magnitudes $\left|E_{SA1,20}(t)\right|^2$ [6]:

$$\frac{|E_{SA10}(t)|^2}{\omega_1} + \frac{|E_{SA20}(t)|^2}{\omega_2} = const = I_0 \tag{40}$$

We introduce the dimensionless quantities

$$I_{1,2}(t) = \frac{|E_{SA1,20}(t)|^2}{\omega_{1,2} I_0}; \;\; I_1(t) + I_2(t) = 1 \tag{41}$$

Substituting relationship (41) into Eq. (36), we obtain

$$\frac{\partial I_{1,2}}{\partial t} = \mp g I_1 I_2 \tag{42}$$

where the gain g has the form

$$g = \frac{8\varepsilon_0 \mathrm{Im} G\left(k_x, k_z^S, \Delta\omega\right) k_x^2 h\left(k_z^S\right)^2 \omega_1 \omega_2 I_0}{\varepsilon_\perp \left|G\left(k_x, k_z^S, \Delta\omega\right)\right|^2} F_N\left(k_x, k_z^S\right) \tag{43}$$

The spectral dependence of the gain g is shown in **Figure 8**. The solution of Eq. (41) has the form

$$I_1(t) = \frac{I_1(0)\exp(-gt)}{1 - I_1(0)[1 - \exp(-gt)]} \tag{44}$$

$$I_2(t) = \frac{1 - I_1(0)}{1 - I_1(0)[1 - \exp(-gt)]} \tag{45}$$

It is easy to see from Eqs. (44) and (45) that the solutions $I_{1,2}(t)$ satisfy the Manley-Rowe relation (40). Expressions (44) and (45) describe the energy

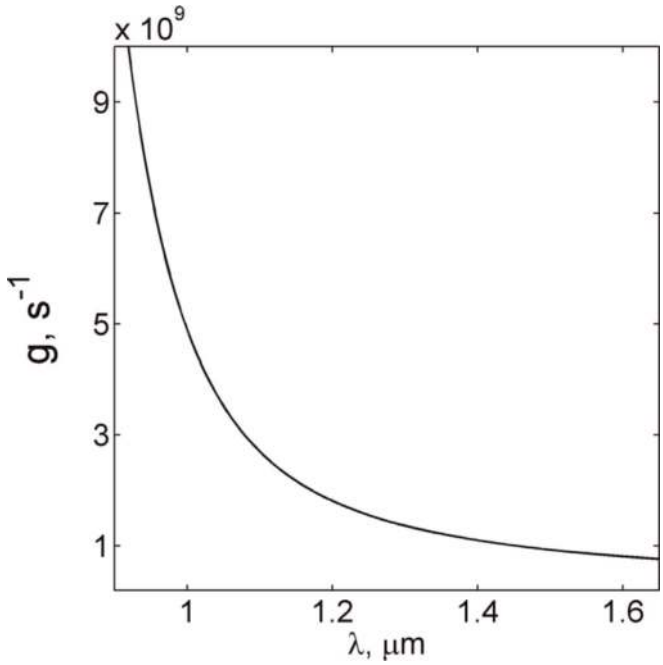

Figure 8.
The spectral dependence of the gain g *for the SPP electric field amplitude* $|E_{SA10}(t)| = 10^6 V/m$.

exchange between the SPPs interfering on the smectic layer dynamic grating. Indeed, $I_1 \to 0$ and $I_2 \to 1$ for $g > 0$ and $t \to \infty$. Actually, the SLS of the orientational type takes place [6]. The SPP_1 with the normalized intensity I_1 plays a role of the pumping wave, while the SPP_2 is a signal wave. The temporal dependence of $I_{1,2}(t)$ for the pumping wave amplitude $|E_{SA10}(t)| = 10^6 V/m$ is shown in **Figure 9**.

It is seen form **Figure 6** that for $I_1(0) > I_2(0)$, the characteristic time t_0 exists when $I_1(t_0) = I_2(t_0)$. Using expressions (44) and (45), we obtain

$$t_0 = \frac{1}{g} \ln \left[\frac{I_1(0)}{I_2(0)} \right] \tag{46}$$

Substitute expression (46) into Eqs. (44) and (45). Then they take the form

$$I_{1,2}(t) = \frac{1}{2} \left[1 \mp \tanh \left[\frac{g}{2} (t - t_0) \right] \right] \tag{47}$$

The time duration of the energy exchange between the SPPs is about $1ns$ as it is seen from **Figure 9**. Substituting relationships (43)–(45) into Eq. (37), we evaluate the phases $\theta_{SA1,2}(t)$. They are given by the following expressions:

$$\theta_{SA1}(t) - \theta_{SA1}(0) = -\frac{\mathrm{Re}\, G\left(k_x, k_z^S, \Delta\omega\right)}{2\mathrm{Im}G\left(k_x, k_z^S, \Delta\omega\right)} \times \ln \left[I_2(0) \exp(gt) + I_1(0) \right] \tag{48}$$

$$\theta_{SA2}(t) - \theta_{SA2}(0) = \frac{\mathrm{Re}\, G\left(k_x, k_z^S, \Delta\omega\right)}{2\mathrm{Im}G\left(k_x, k_z^S, \Delta\omega\right)} \times \ln \left[1 - I_1(0) + I_1(0) \exp(-gt) \right] \tag{49}$$

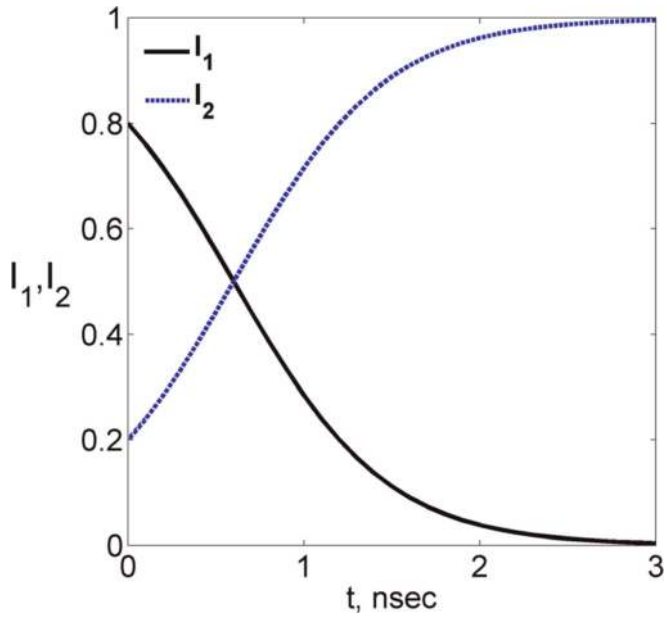

Figure 9.
The temporal dependence of the SPP normalized intensities $I_{1,2}(t)$ for pumping wave amplitude $|E_{SA10}(t)| = 10^6 V/m$.

The temporal dependence of the SPP SVA phases $\theta_{SA1,2}(t)$ is shown in **Figure 10**.

It is seen from expressions (48) and (49) that SLS of the SPPs in the MIM waveguide is accompanied by XPM. For the large time intervals $t \to \infty$, the phase of the pumping wave increases linearly:

$$\theta_{SA1}(t) - \theta_{SA1}(0) \to -\frac{\mathrm{Re}\, G\left(k_x, k_z^S, \Delta\omega\right)}{2\mathrm{Im}G\left(k_x, k_z^S, \Delta\omega\right)} gt \tag{50}$$

Such a behavior corresponds to the rapid oscillations of the depleted pumping wave amplitude. The signal wave phase for $t \to \infty$ tends to a constant value:

$$\theta_{SA2}(t) - \theta_{SA2}(0) \to \frac{\mathrm{Re}\, G\left(k_x, k_z^S, \Delta\omega\right)}{2\mathrm{Im}G\left(k_x, k_z^S, \Delta\omega\right)} \ln\left[1 - I_1(0)\right] \tag{51}$$

Substituting expressions (41) and (47) into Eq. (29), we obtain the explicit expression for the dynamic grating amplitude. It takes the form

$$U_0 = -\frac{2\varepsilon_0 I_0 k_x^2 k_z^S \sqrt{\omega_1\omega_2} h}{G\left(k_x, k_z^S, \Delta\omega\right) \cosh\left[\frac{g}{2}(t - t_0)\right]} \exp i(\theta_{SA1} - \theta_{SA2}) \tag{52}$$

The temporal dependence of the amplitude (52) normalized absolute value $|U_0/U_{0\max}|$ is presented in **Figure 11**. Here

$$|U_{0\max}| = \frac{2\varepsilon_0 I_0 \left|k_x^2 k_z^S\right| \sqrt{\omega_1\omega_2} |h|}{\left|G\left(k_x, k_z^S, \Delta\omega\right)\right|} \tag{53}$$

We evaluate now the hydrodynamic flow velocity in the MIM wave guide core. Substituting expression (28) into Eqs. (1) and (6), we obtain

$$v_z(x, z, t) = -i\Delta\omega U_0 \sinh\left(2k_z^S z\right) \exp\left[i(2k_x x - \Delta\omega t)\right] + c.c. \tag{54}$$

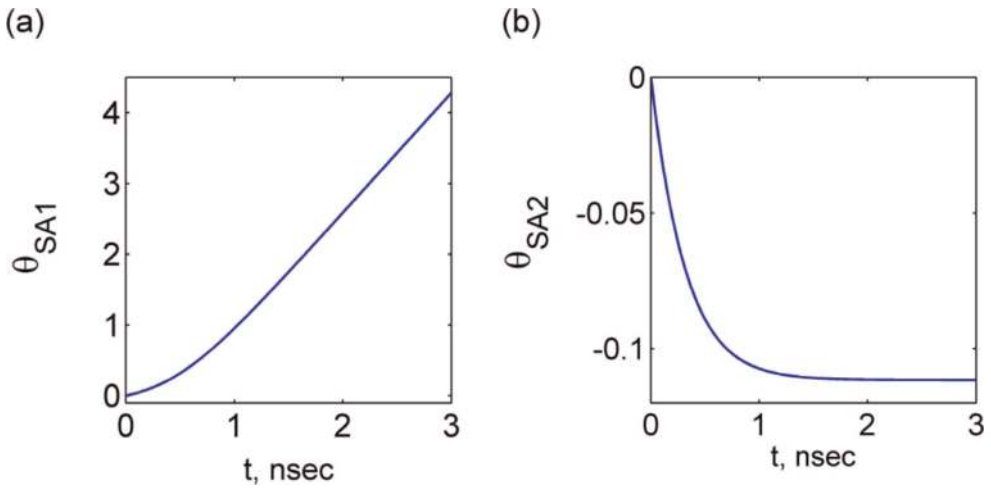

Figure 10.
The temporal dependence of the SPP SVA phases $\theta_{SA1}(t)$ (a) and $\theta_{SA2}(t)$ (b).

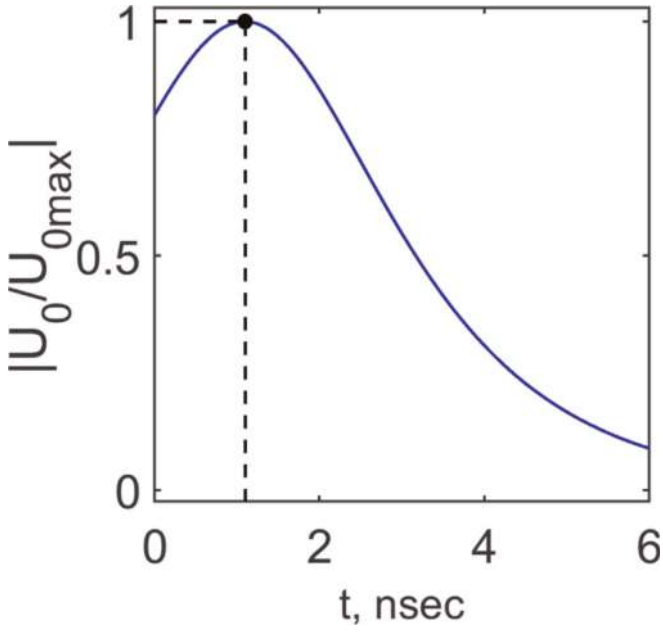

Figure 11.
The temporal dependence of the dynamic grating amplitude normalized absolute value $|U_0/U_{0\max}|$.

$$v_x(x,z,t) = \Delta\omega U_0 \frac{k_z^S}{k_x} \cosh\left(2k_z^S z\right) \exp\left[i(2k_x x - \Delta\omega t)\right] + c.c. \tag{55}$$

Expressions (28) and (52)–(55) and **Figure 11** show that the orientational and hydrodynamic excitations in SmALC core of the MIM waveguide enhanced by the SPPs are spatially localized and reach their maximum value during the time of the energy exchange between the interacting SPPs.

5. Conclusions

We investigated theoretically the nonlinear interaction of SPPs in the MIM waveguide with the SmALC core. The third-order nonlinearity mechanism is related to the smectic layer oscillations that take place without the change of the mass density. We solved simultaneously the equation of motion for the smectic layer normal displacement and the Maxwell equations for SPPs including the nonlinear polarization caused by the smectic layer strain. We evaluated the dynamic grating of the smectic layer displacement enhanced by the interfering SPPs. We evaluated the SVAs of the interacting SPPs. It has been shown that the SLS of the orientational type takes place. The pumping wave is depleted, while the signal wave is amplified up to the saturation level defined by the total intensity of the interacting waves. SLS is accompanied by XPM. The phase of the depleted pumping wave rapidly increases, while the phase of the amplified wave tends to a constant value. The SPP characteristic rise time is of the magnitude of 10^{-9} s for a feasible SPP electric field of 10^6 V/m. The smectic layer displacement and hydrodynamic velocity enhanced by SPPs are spatially localized and reach their maximum value during the time of the strong energy exchange between the interfering SPPs.

Author details

Boris I. Lembrikov*, David Ianetz and Yossef Ben Ezra
Department of Electrical Engineering and Electronics, Holon Institute of Technology (HIT), Holon, Israel

*Address all correspondence to: borisle@hit.ac.il

References

[1] Kauranen M, Zayats AV. Nonlinear plasmonics. Nature Photonics. 2012;**6**: 737-748. DOI: 10.1038/NPHOTON.2012.244

[2] Willner AE, Yilmaz OF, Wang J, Wu X, Bogoni A, Zhang L, et al. Optically efficient nonlinear signal processing. IEEE Journal of Selected Topics in Quantum Electronics. 2011;**17**: 320-332. DOI: 10.1109/JSTQE.2010.2055551

[3] Willner AE, Khaleghi S, Chitgarha MR, Yilmaz OF. All-optical signal processing. Journal of Lightwave Technology. 2014;**32**:660-680. DOI: 10.1109/JLT.2013.2287219

[4] Gai X, Choi D-Y, Madden S, Luther-Davies B. Materials and structures for nonlinear photonics. In: Wabnitz S, Eggleton BJ, editors. All-Optical Signal Processing. Heidelberg: Springer; 2015. pp. 1-33. DOI: 10.1007/978-3-319-14992-9

[5] Kik PG, Brongersma ML. Surface plasmon nanophotonics. In: Brongersma ML, Kik PG, editors. Surface Plasmon Nanophotonics. Dordrecht: Springer; 2007. pp. 1-9. ISBN: 978-1-4020-4349-9

[6] Shen YR. The Principles of Nonlinear Optics. Hoboken. New Jersey, USA: Wiley; 2003. p. 563. ISBN: 0-471-43080-3

[7] Maier SA. Plasmonics: Fundamentals and Applications. New York: Springer; 2007. p. 223. ISBN: 978-0387-33150-8

[8] Sarid D, Challener W. Modern Introduction to Surface Plasmons. Cambridge: Cambridge University Press; 2010. 371 p. ISBN: 978-0-521-76717-0

[9] Sederberg S, Firby CJ, Greig SR, Elezzabi AY. Integrated nanoplasmonic waveguides for magnetic, nonlinear, and strong-field devices. Nanophotonics. 2017;**6**:235-257. DOI: 10.1515/nanoph-2016-0135

[10] Lapine M. Colloquium: Nonlinear metamaterials. Reviews of Modern Physics. 2014;**86**:1093-1123. DOI: 10.1103/RevModPhys.86.1093

[11] Zheludev NI, Kivshar YS. From metamaterials to metadevices. Nature Materials. 2012;**11**:917-924. DOI: 10.1038/NMAT3431

[12] Khoo IC. Nonlinear optics, active plasmonics and metamaterials with liquid crystals. Progress in Quantum Electronics. 2014;**38**:77-117. DOI: 10.1016/j.pquantelec.2014.03.001

[13] Khoo IC. Nonlinear optics of liquid crystalline materials. Physics Reports. 2009;**471**:221-267. DOI: 10.1016/j.physrep.2009.01.001

[14] Khoo I-C. Liquid Crystals. 2nd ed. Hoboken, New Jersey, USA: Wiley; 2007. p. 368. ISBN 978-0-471-75153-3

[15] Giallorenzi TG, Weiss JA, Sheridan JP. Light scattering from smectic liquid-crystal waveguides. Journal of Applied Physics. 1976;**47**: 1820-1826. DOI: 10.1063/1.322898

[16] Kventsel GF, Lembrikov BI. Two-wave mixing on the cubic non-linearity in the smectic A liquid crystals. Liquid Crystals. 1994;**16**:159-172. ISSN: 0267-8292

[17] Kventsel GF, Lembrikov BI. Stimulated light scattering in smectic A liquid crystals. Liquid Crystals. 1995;**19**: 21-37. ISSN: 0267-8292

[18] Kventsel GF, Lembrikov BI. Self-focusing and self-trapping in smectic A liquid crystals. Molecular Crystals and

Liquid Crystals. 1995;**262**:629-643. ISSN: 1542-1406

[19] Kventsel GF, Lembrikov BI. The four-wave mixing and the hydrodynamic excitations in smectic A liquid crystals. Molecular Crystals and Liquid Crystals. 1995;**262**:591-627. ISSN: 1542-1406

[20] Kventsel GF, Lembrikov BI. Second sound and nonlinear optical phenomena in smectic A liquid crystals. Molecular Crystals and Liquid Crystals. 1996;**282**: 145-189. ISSN: 1542-1406

[21] Lembrikov BI. Light interaction with smectic A liquid crystals: Nonlinear effects. HAIT Journal of Science and Engineering. 2004;**1**:306-347. ISSN: 1565-4990

[22] Lembrikov BI, Ben-Ezra Y. Surface plasmon polariton (SPP) interactions at the interface of a metal and smectic liquid crystal. In: Proceedings of the 17th International Conference on Transparent Optical Networks (ICTON 2015); July 5-9, 2015; Budapest, Hungary (We.C4.4). 2015. pp. 1-4

[23] Lembrikov BI, Ben-Ezra Y, Ianetz D. Stimulated scattering of surface plasmon polaritons (SPPs) in smectic A liquid crystal. In: Proceedings of the 18th International Conference on Transparent Optical Networks (ICTON-2016); July 10-14, 2016; Trento, Italy (We.B4.2). 2016. pp. 1-4

[24] Lembrikov BI, Ianetz D, Ben-Ezra Y. Metal/insulator/metal (MIM) plasmonic waveguide containing a smectic A liquid crystal (SALC) layer. In: Proceedings of the 19th International Conference on Transparent Optical Networks (ICTON 2017); July 2-6, 2017; Girona, Catalonia, Spain (Tu.A4.3). 2017. pp. 1-4

[25] Lembrikov BI, Ianetz D, Ben-Ezra Y. Nonlinear optical phenomena in silicon-smectic A liquid crystal (SALC) waveguiding structures. In: Proceedings of the 20th Int'l. Conf. on Transparent Optical Networks (ICTON 2018), 1-5 July 2018 Bucharest, Romania (Mo. D4.1). 2018. pp. 1-4

[26] Lembrikov BI, Ianetz D, Ben-Ezra Y. Nonlinear optical phenomena in smectic A liquid crystals. In: Choudhury PK, editor. Liquid Crystals—Recent Advancements in Fundamental and Device Technologies. Rijeka, Croatia: InTechOpen; 2018. pp. 131-157. DOI: 10.5772/intechopen.70997

[27] Lembrikov BI, Ianetz D, Ben-Ezra Y. Nonlinear optical phenomena in a silicon-smectic A liquid crystal (SALC) waveguide. Materials. 2019;**12**:2086-1-2086-17. DOI: 10.3390/ma12132086

[28] Lembrikov BI, Ianetz D, Ben-Ezra Y. Light enhanced flexoelectric polarization in waveguiding structures with a smectic A liquid crystal (SALC) layer. In: Proceedings of the 20th International Conference on Transparent Optical Networks (ICTON 2019); 9-13 July 2019; Angers, France, Th.B4.3. 2019. pp. 1-4

[29] De Gennes PG, Prost J. The Physics of Liquid Crystals. 2nd ed. New York, USA: Oxford University Press; 1993. 597 p. ISBN: 978-0198517856

[30] Stephen MJ, Straley JP. Physics of liquid crystals. Reviews of Modern Physics. 1974;**46**:617-704. ISSN: 0034-6861

[31] Chandrasekhar S. Liquid Crystals. 2nd ed. Cambridge: Cambridge University Press; 1992. p. 480. ISBN: 978-0521427418

[32] Liao Y, Clark NA, Pershan PS. Brillouin scattering from smectic liquid crystals. Physical Review Letters. 1973; **30**:639-641. DOI: 10.1103/PhysRevLett. 30.639

[33] Ricard L, Prost J. "Second sound" propagation and the smectic response function. Journal DE Physique Colloque C3. 1979;**40**(supplement 4): C3-83-C3-86. DOI: 10.1051/jphyscol: 1979318

[34] Ricard L, Prost J. Critical behavior of second sound near the smectic A nematic phase transition. Journal De Physique. 1981;**42**:861-873. DOI: 10.1051//jphys:01981004206086100

[35] Zografopoulos DC, Asquini R, Kriezis EE, d'Alessandro A, Becceherelli R. Guided-wave liquid-crystal photonics. Lab on a Chip. 2012; **12**:3598-3610. DOI: 10.1039/c21c40514h

[36] Zografopoulos DC, Becceherelli R, Tasolamprou AC, Kriezis EE. Liquid-crystal tunable waveguides for integrated plasmonic components. Photonics and Nanostructures-Fundamentals and Applications. 2013; **11**:73-84. DOI: 10.1016/j.photonics. 2012.08.004

[37] Zografopoulos DC, Beccherelli R. Liquid-crystal-tunable metal-insulator-plasmonic waveguides and Bragg resonators. Journal of Optics. 2013;**15**: 1-5. DOI: 10.1088/2040-8978/15/5/ 055009

[38] Prokopidis KP, Zografopoulos DC, Kriezis EE. Rigorous broadband investigation of liquid-crystal plasmonic structures using finite-difference time-domain dispersive-anisotropic models. Journal of the Optical Society of America B. 2013;**30**(10):2722-2730. DOI: 10.1364/JOSAB.30.002722

[39] Ma L-L, Hu W, Zheng Z-G, Wu S-B, Chen P, Li Q, et al. Light-activated liquid crystalline hierarchical architecture toward photonics. Advanced Optical Materials. 2019; **1900393**:1-19. DOI: 10.1002/adom. 201900393

[40] Suhara T, Fujimura M. Waveguide Nonlinear-Optic Devices. Berlin, Germany: Springer; 2003. p. 321. ISBN: 3-540-01527-2